Journal of Structural Geology 31 (2009) 1197–1211

Contents lists available at ScienceDirect

Journal of Structural Geology

journal homepage: www.elsevier.com/locate/jsg

Kinematic significance of L tectonites in the footwall of a major terrane-bounding thrust fault, Klamath Mountains, California, USA

W.A. Sullivan*

Department of Geology, Colby College, 5803 Mayflower Hill, Waterville, ME 04901, USA

ARTICLE INFO

Article history:
Received 13 January 2009
Received in revised form
23 May 2009
Accepted 29 June 2009
Available online 8 July 2009

Keywords:
L tectonites
Constriction
Constrictional strain
Shear zone
Klamath Mountains
Western Hayfork terrane

ABSTRACT

Detailed geologic mapping, cross-section reconstructions, strain analyses, and kinematic analyses, enable the reconstruction of a ~one-kilometer-wide domain of L tectonites in the east–west-striking, sub-horizontal to gently south-dipping Pigeon Point high-strain zone (PPHSZ) associated with a major thrust fault separating oceanic- and arc-affinity terranes in the Klamath Mountains, California. L tectonites are associated with: (1) a convex-upward warp of the upper high-strain-zone boundary, (2) a transition from mafic metavolcaniclastic rocks to micaceous quartzites, (3) folds subparallel with mineral lineations, (4) emplacement of synkinematic ultramafic/mafic intrusive bodies, and (5) a local temperature increase from greenschist- to amphibolite-facies conditions. Pure-shear-dominated deformation accommodated zone-normal shortening and transport-parallel elongation coupled with subordinate top-to-the-west-directed, thrust-style simple shear. L tectonite formation was controlled by the shape of the high-strain-zone boundary driving lateral flow into the apex of the lens-shaped zone in response to a favorable kinematic geometry and bulk strain in the constrictional field. Localized magmatic heating best explains the shape of the high-strain-zone boundary, but L tectonites are not partitioned into a single rheological domain. During terrane amalgamation strain-path partitioning occurred with localized top-to-the-west-directed simple shear partitioned into a structurally overlying thrust zone and pure-shear-dominated subvertical shortening and transport-parallel elongation partitioned into the PPHSZ.

1. Introduction

Lateral accretion at subduction margins is an important and widely recognized mechanism of continental growth, and belts of oceanic-, arc-, and continental-affinity accreted terranes are found in orogenic systems ranging in age from Archean to modern (e.g. Condie, 1982; Plafker et al., 1989; Robinson et al., 1998; Huang et al., 2000; Snoke et al., 2001; Schmid et al., 2004; Frost et al., 2006; Dickinson, 2008). In many cases, however, the exact mechanisms of terrane amalgamation and accretion remain enigmatic. In some orogenic belts terranes are partially or completely subducted only to be exhumed and exposed as fault slices (e.g. Schmid et al., 1996). Elsewhere accreted supra-crustal material is left unmetamorphosed or subjected to only low-pressure metamorphism associated with mid- to upper-crustal arc magmatism (e.g. Frost et al., 2006; Gerbi and West, 2007). In most all cases only slices and dismembered fragments of what were once large crustal blocks are exposed, leading to extreme telescoping of past plate-tectonic systems (e.g. Robinson et al., 1998; Schmid et al., 2004; Dickinson, 2008). Moreover, in many cases terrane-bounding fault systems are overprinted by stitching plutons and/or highly modified by later deformation, and the nature of deformation accommodating the initial dismemberment and subsequent reassembly of telescoped crustal fragments is unknown.

To some degree this lack of understanding of the mechanisms leading to crustal dismemberment and the subsequent formation of belts of highly telescoped accreted terranes is related to our limited understanding of how and why deformation is partitioned in the middle and lower crust. Historically plastic high-strain zones were interpreted in two dimensions using a model of progressive simple-shear deformation (Ramsay and Graham, 1970). However, case studies of natural high-strain zones tell us that non-plane-strain deformation is common (e.g. Pfiffner and Ramsay, 1982 their Fig. A1) and that strict monoclinic simple-shear deformation is the exception rather than the rule (e.g. Lin and Jiang, 2001; Bailey et al., 2004; Giorgis and Tikoff, 2004). Structural interpretations are further complicated by high-strain zones that are non-planar and/or contain complex internal rheological and kinematic domains. Complex spatial variations in strain geometry and strain path are found in a wide variety structural settings and plate-tectonic

* Tel.: +1 207 859 5803; fax: +1 207 859 5868.
E-mail address: wasulliv@colby.edu

0191-8141/$ – see front matter © 2009 Elsevier Ltd. All rights reserved.
doi:10.1016/j.jsg.2009.06.016

environments including transpressional shear zones (e.g. Goodwin and Williams, 1996; Czeck and Hudleston, 2003; Sullivan and Law, 2007), footwall shear zones of metamorphic core complexes (e.g. Bailey and Eyster, 2003; Sullivan, 2008), and shallowly dipping high-strain zones in contractional orogenic systems (e.g. Law et al., 1984; Xypolias and Koukouvelas, 2001; Jessup et al., 2006). Interpreting these complex spatial kinematic and strain variations is an important step in understanding how deformation is accommodated in the middle and lower crust. Perhaps the most enigmatic of these internal strain variations is the formation of large domains of constrictional strain often manifested by pure or nearly pure linear fabrics, or L tectonites (Flinn, 1965). Domains of L tectonites associated with continental growth by amalgamation of oceanic-, arc-, and continental-affinity terranes are found in a number of orogenic belts world wide (e.g. Wright and Fahan, 1988; Brown and Talbot, 1989; Flinn, 1992; Hacker and Mosenfelder, 1996; Lin and Jiang, 2001; Snoke et al., 2001; Kurz, 2005), but the exact kinematic significance of constrictional deformation associated with terrane amalgamation at convergent margins is often incompletely understood. Therefore, to improve our understanding of both the kinematic significance of L tectonites within major high-strain zones and the nature of deformation leading to the formation of telescoped belts of accreted terranes I present a detailed case study of a one-kilometer-wide domain of L tectonites in a subhorizontal to gently dipping high-strain zone associated with a major thrust-fault system separating oceanic- and arc-affinity terranes in the Klamath Mountains, California, referred to as the Pigeon Point high-strain zone (PPHSZ). These data and analyses enable two important conclusions. First, the formation of L tectonites in the PPHSZ is associated with a variation in the shape of the high-strain-zone boundary, localized magmatic heating, and a bulk kinematic geometry favorable for the localization of constrictional strain. Second, the PPHSZ developed in response to vertical shortening related to contractional deformation and thrust loading during terrane amalgamation, but it is not a simple-shear-dominated, terrane-bounding fault zone. Simple-shear deformation related to terrane emplacement was partitioned into a structurally overlying thrust-fault zone. These results provide a better understanding of how and why constrictional fabrics form in high-strain zones, and will help future geologists encountering L tectonites in the field to better interpret them. Moreover, because they provide a detailed description of strain partitioning and plastic deformation during the amalgamation of two major oceanic- and arc-affinity accreted terranes, they also improve our understanding of how and why strain is partitioned during lateral terrane accretion and continental growth.

2. Regional geologic setting

2.1. The Klamath Mountains province

The Klamath Mountains province in northwestern California and southwestern Oregon is constructed of assemblages of oceanic- and arc-affinity rocks that were accreted onto the western margin of North America during subduction-related processes, manifested by a long-lived history (>400 m.y.) of tectonic growth (Irwin, 1981, 1994; Snoke and Barnes, 2006). Irwin (1960) first recognized that the province can be divided into roughly north–south-striking lithic belts and initially defined, from east-to-west, the eastern Klamath, central metamorphic, western Paleozoic and Triassic, and western Jurassic belts. Subsequently a number of authors further subdivided these four lithic belts into a series of distinct fault-bounded tectonostratigraphic terranes (e.g. Davis et al., 1965; Irwin, 1972, 1994; Wright, 1982; Harper, 1984; see also Snoke and Barnes, 2006 for an overview of the terrane concept in the Klamath Mountains province). Terranes exposed in the southern Klamath Mountains in the area of this study (Fig. 1) include, from east-to-west, the central metamorphic and Stuart Fork terranes of the original central metamorphic belt (Davis et al., 1965; Goodge, 1989a,b; Peacock and Norris, 1989; Barrow and Metcalf, 2006); the North Fork, eastern Hayfork, western Hayfork, and Rattlesnake Creek terranes of the original western Paleozoic and Triassic belt (Irwin, 1972; Wright, 1982; Ando et al., 1983; Ernst et al., 1991; Ernst, 1999); and the Smith River subterrane (specifically, the Galice Formation and Devil's Elbow ophiolite remnant) of the original western Jurassic belt (Garcia, 1979; Harper, 1984; Wyld and Wright, 1988; Harper et al., 1994).

The Stuart Fork, North Fork, and eastern Hayfork terranes (Fig. 1) comprise a genetically related accretionary complex/fore-arc assemblage that was formed and amalgamated during late Paleozoic–early Mesozoic accretion (Wright, 1982; Ando et al., 1983; Ernst et al., 1991; Ernst, 1999). The Stuart Fork terrane experienced metamorphism under blueschist-facies conditions during the Late Triassic and represents exhumed, partially subducted oceanic sedimentary and volcanic rocks (Hotz et al., 1977; Goodge, 1989a,b; Ernst, 1999). The North Fork terrane is composed of a supra-subduction-zone ophiolite on which Permian? and Triassic arc tholeiites were erupted (Ando et al., 1983; Ernst et al., 1991; Ernst, 1999). The eastern Hayfork terrane is composed of argillite-matrix mélange and broken formation that contains early Mesozoic radiolarians (Irwin et al., 1977; Wright, 1982; Ando et al., 1983).

The eastern Hayfork terrane is structurally underlain by calc-alkaline volcanogenic sandstones and breccias and interbedded epiclastic and hemipelagic sedimentary rocks that collectively comprise the western Hayfork terrane (Fig. 1) (Irwin, 1972, 1994; Wright, 1982; Wright and Fahan, 1988). Volcanic clasts and crystal fragments from volcanogenic sandstones and breccias of the western Hayfork terrane yielded ages of 168 ± 1.9 Ma, 171 ± 2.0 Ma, and 177 ± 2.8 Ma (K–Ar, hornblende) (Wright and Fahan, 1988), and Donato et al. (1996) reported 172.3 ± 1.0 and 173.3 ± 1.3 Ma ($^{40}Ar/^{39}Ar$, hornblende) magmatic ages from correlative rocks exposed in the northern Klamath Mountains. These rocks are interpreted to represent the remnants of a Middle Jurassic volcanic arc, the western Hayfork arc (Wright, 1982; Wright and Fahan, 1988).

The Rattlesnake Creek terrane structurally underlies the western Hayfork terrane (Fig. 1) and is composed of a serpentinite-matrix ophiolitic mélange that is intruded and overlain by a Late Triassic–Early Jurassic volcanic-arc sequence (Wright, 1982; Donato, 1987; Wright and Fahan, 1988; Wright and Wyld, 1994; Irwin, 1994). Wright and Wyld (1994) interpret the Triassic–Jurassic arc sequence of the Rattlesnake Creek terrane as exotic based on its position outboard of the well-defined, contemporaneous Stuart Fork/North Fork/eastern Hayfork accretionary complex/fore-arc assemblage. The Rattlesnake Creek terrane likely forms part of the basement upon which the western Hayfork arc was built (Wright and Fahan, 1988).

2.2. Middle Jurassic deformation and metamorphism

The Jurassic–Early Cretaceous history of the Klamath Mountains province is characterized by nearly continuous arc magmatism and alternating episodes of contractional and extensional deformation associated with regional metamorphism (Wright, 1982; Wright and Fahan, 1988; Harper et al., 1990, 1994; Hacker et al., 1995; Allen and Barnes, 2006). Because the rocks cut by the PPHSZ are part of the western Hayfork terrane and have Middle Jurassic protolith ages and deformation in this zone is of Middle Jurassic age, this discussion is limited to Middle Jurassic deformation and metamorphic events. During the Middle Jurassic, the central

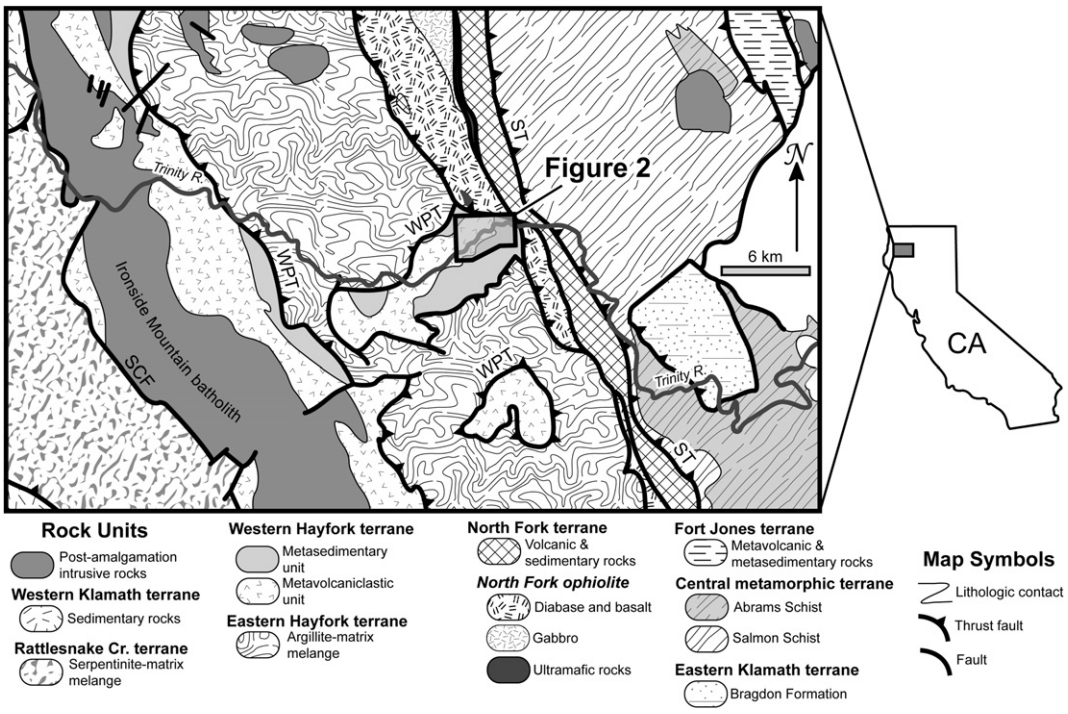

Fig. 1. Geologic sketch map of the southeastern Klamath Mountains, California (after Irwin, 1994) showing the locations of terranes discussed in the text and the area of Fig. 2. SCF = Salt Creek fault, ST = Siskyou thrust, and WPT = Wilson Point thrust.

metamorphic, Stuart Fork, North Fork, eastern Hayfork, western Hayfork, and Rattlesnake Creek terranes were imbricated along a series of east-dipping, low-angle faults widely interpreted as thrust faults (Davis et al., 1965; Davis, 1968; Wright, 1982; Hill, 1985; Wright and Fahan, 1988). Specifically, the central metamorphic terrane is separated from the Stuart Fork and North Fork terranes by the Siskiyou thrust (Davis et al., 1965; Davis, 1968), the eastern Hayfork terrane is separated from the western Hayfork terrane by the Wilson Point thrust (Wright, 1982), and the western Hayfork terrane is separated from the Rattlesnake Creek terrane by the Salt Creek fault (Wright, 1982; Wright and Fahan, 1988). In the area of this study, the Wilson Point thrust accommodated a minimum of 13 km of heave (Fig. 1) (Irwin, 1994). North of the area of this study, Donato (1987) interpreted the contact between the western Hayfork and Rattlesnake Creek terranes as a faulted depositional contact. In many localities, low-angle faults were extensively modified by later high-angle normal faulting. This Middle Jurassic contractional event is associated with regional greenschist- to amphibolite-facies metamorphism and penetrative deformation and is collectively referred to as the Siskiyou event (Coleman et al., 1988; Wright and Fahan, 1988). Lower age bounds for the Wilson Point thrust and the Salt Creek fault are provided by the 177–168-Ma igneous crystallization ages of hornblendes collected from the western Hayfork terrane. These faults are overprinted by the ~170-Ma (U-Pb zircon, Wright and Fahan, 1988) Ironside Mountain batholith (Fig. 1), and contact metamorphism associated with the intrusion of this composite pluton overprints penetrative deformation fabrics that are coeval with regional metamorphism in the Rattlesnake Creek, western Hayfork, and eastern Hayfork terranes (Barnes et al., 2006). The ages of both the Wilson Point thrust and Salt Creek fault are therefore bracketed at ~170 Ma by the errors in the available geochronology, and these structures must be nearly coeval with the Middle Jurassic arc volcanism recorded by the western Hayfork terrane (Barnes et al., 2006).

3. Local geologic setting and unit descriptions

3.1. Local setting of the Pigeon Point high-strain zone

The PPHSZ is an east–west-striking, subhorizontal to gently south-dipping structure that cuts part of the western Hayfork terrane exposed in a window through the structurally overlying eastern Hayfork terrane and Wilson Point thrust in the area of Pigeon Point along the Trinity River (Figs. 1 and 2). Wright (1982) and Wright and Fahan (1988) outlined a coherent stratigraphic succession in the western Hayfork terrane. Rock units cut by the PPHSZ include a structurally lower unit comprised of metamorphosed mafic volcaniclastic tuff breccias and volcanogenic sandstones hereon referred to as the metavolcaniclastic unit and an overlying metamorphosed sequence of argillite and chert that locally includes lesser amounts of sandstone and conglomerate hereon referred to as the metasedimentary unit. Both of these units underwent regional metamorphism under greenschist-facies conditions and contain a weak foliation. Composite clinopyroxenite/hornblende-gabbro dikes intrude the metavolcaniclastic and metasedimentary units at Pigeon point (Fig. 2), and these bodies are associated with an increase in metamorphic temperatures from greenschist- to amphibolite-facies conditions (Wright and Fahan, 1988).

3.2. Metavolcaniclastic unit

In the area of this study, the metavolcaniclastic unit includes massive mafic tuff breccias, crystal-lithic tuffs, and volcanogenic lithic sandstones deposited by subaqueous debris flows and turbidity currents from a proximal volcanic arc (Wright and Fahan, 1988). Clasts in tuff breccias range from 1 to 30 cm in diameter, and they are dominated by porphyritic lava fragments with locally significant pumiceous clasts (Fig. 3) (Wright and Fahan, 1988). Clasts and the surrounding matrix typically contain the same mineral assemblage with only minor differences in modal composition. Throughout the study area, the

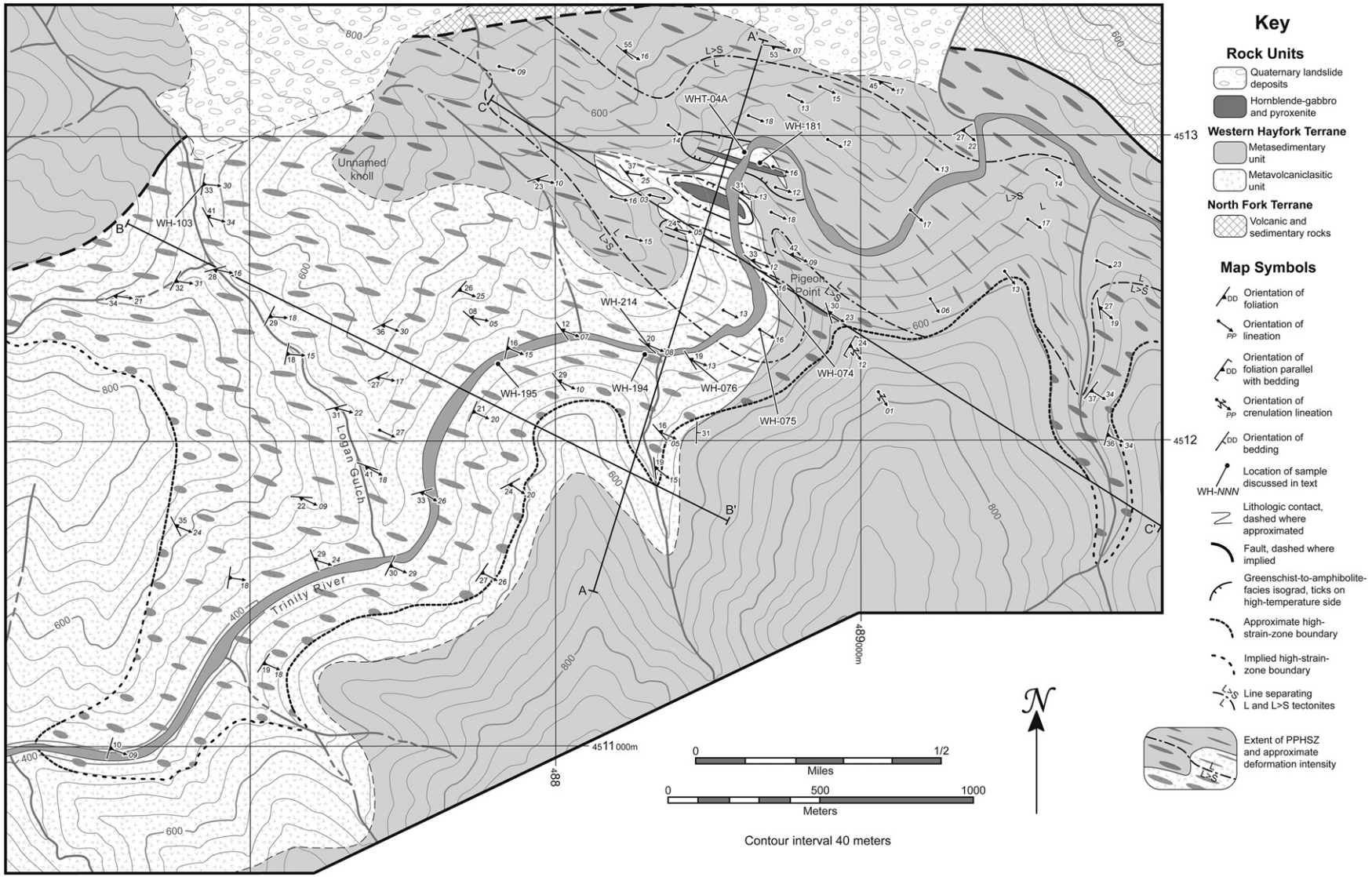

Fig. 2. Geologic map of the Pigeon Point high-strain zone (PPHSZ) showing the domain of L tectonites; the high-strain-zone boundary; the locations of strain analyses and oriented samples discussed in the text and presented in Figs. 3–5 and 8; and locations of cross sections in Fig. 7. Contacts outside of the PPHSZ are modified from Fahan (1982). The pattern of ellipses within the PPHSZ is generalized and intended to show the approximate shape of finite-strain ellipsoids viewed down into the ground on lineation-parallel faces.

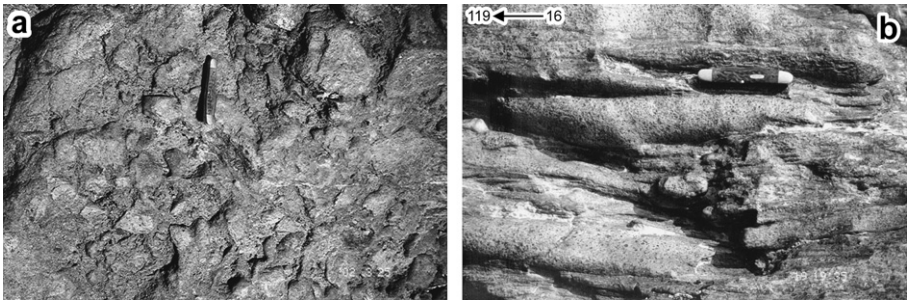

Fig. 3. (a) Undeformed tuff-breccia clasts in the metavolcaniclastic unit exposed along the Trinity River near the area of this study. Location of photo is outside of the area of Fig. 2. (b) Cigar-shaped deformed tuff-breccia clasts in the domain of L tectonites. Photograph was taken at locality WH-074 (Figs. 2 and 5). View is straight down on a lineation-parallel face. Orientation of the mineral lineation and the long axes of the clasts is indicated in the upper left-hand corner of the photo. Knife used for scale is 9.8-cm long.

metavolcaniclastic unit was pervasively metamorphosed under greenschist-facies conditions and contains the characteristic metamorphic mineral assemblage blue-green actinolite + green actinolite + epidote + biotite + quartz ± chlorite ± carbonate minerals. Outside of the PPHSZ, original pyroxene and hornblende phenocrysts are commonly well preserved, and plagioclase phenocrysts, though altered, are readily distinguished. In the PPHSZ, pyroxene and hornblende phenocrysts are almost entirely psuedomorphed by actinolite, and plagioclase is rarely observed. The matrix surrounding the phenocrysts is composed of a fine-grained aggregate of epidote, actinolite needles, quartz, and local chlorite. Actinolite in the matrix and actinolite pseudomorphs of hornblende phenocrysts exhibit green pleochroism, whereas actinolite pseudomorphs of pyroxenes commonly exhibit blue-green pleochroism. Blue-green actinolite is sometimes epitaxially overgrown by green actinolite. Within the PPHSZ, quartz and carbonate minerals frequently constitute a significant portion of the matrix. Porphyroclasts (phenocrysts) in the PPHSZ are often rimmed by pressure-shadow overgrowths of quartz and/or carbonate minerals intergrown with actinolite, chlorite, and, in some samples, biotite (Fig. 4c). Deformation-fabric-parallel faces of the porphyroclasts are sometimes rimmed by a thin seam of fine-grained epidote. The pervasive replacement of phenocrysts by metamorphic minerals in the PPHSZ, a complete lack of textural evidence for crystal-plastic deformation in quartz, and the prevalence of metamorphic minerals intergrown with quartz and carbonate minerals in pressure-shadow overgrowths indicate that the dominate deformation mechanism in greenschist-facies tectonites was reaction-assisted diffusive mass transfer.

Wright and Fahan (1988) recognized a small domain of amphibolite-facies metamorphism within the PPHSZ in the L tectonite domain, roughly centered about the clinopyroxenite/hornblende-gabbro dikes exposed at Pigeon Point (Fig. 2). In this area, rocks assigned to the metavolcaniclastic unit include both amphibolite and local garnet amphibolite. Garnet amphibolite contains pods of non-garnetiferous amphibolite that I interpret as relict tuff-breccia clasts. The transition from amphibolite to garnet amphibolite is abrupt, and both rock types are interfolded with each other and the overlying metasedimentary rocks. The inclusion of non-garnetiferous pods within garnet amphibolite and the abrupt transition between the different types of amphibolite indicates that garnet growth in these rocks was likely a function of protolith composition. Deformation fabrics in amphibolites are parallel with those in the enveloping greenschist-facies tectonites. Within amphibolites, hornblende is locally rimmed by actinolite and quartz in the matrix displays subgrain-rotation and minor grain-boundary-migration dynamic recrystallization (regime-II–III transition of Hirth and Tullis, 1992). These observations indicate that the final increments of deformation in these rocks occurred under upper-greenschist-facies conditions. The transition between greenschist- and amphibolite-facies metamorphic assemblages is typically gradational over a distance of 10–50 m or more, but locally it can be quite sharp, occurring over a few meters.

3.3. Metasedimentary unit

The protolith of the metasedimentary unit was predominately siliceous argillite and subordinate interbedded chert. Schists interpreted as metamorphosed graywackes locally crop out near the contact with the metavolcaniclastic unit. Metamorphosed siliceous argillite is ordinarily black on fresh and weathered faces and contains the assemblage quartz + chlorite + white mica + epidote + opaque minerals (graphite?) ± garnet ± biotite. Within the area of amphibolite-facies metamorphism at Pigeon Point, metamorphosed siliceous argillite is noticeably coarser grained and contains the assemblage quartz + biotite + muscovite + garnet ± chlorite. The abundant opaque minerals (graphite?) that give the greenschist-facies rocks a black color in hand sample are not present in the amphibolite-facies rocks, and they are now gray to brown on both fresh and weathered faces. Quartz in greenschist-facies tectonites underwent subgrain-rotation dynamic recrystallization (regime-II of Hirth and Tullis, 1992), whereas quartz in amphibolite-facies samples underwent pervasive grain-boundary-migration dynamic recrystallization (regime-III of Hirth and Tullis, 1992) and often exhibits subpolygonal recrystallized grain shapes (Fig. 4a), indicating a high rate of recovery of intracrystalline strain. One sample of metamorphosed siliceous argillite from the amphibolite-facies domain is intruded by a one-centimeter-wide granitic dike. Feldspars in this dike underwent extensive subgrain-rotation dynamic recrystallization and quartz exhibits pervasive grain-boundary-migration recrystallization (regime-III of Hirth and Tullis, 1992). These observations indicate an increase in deformation temperature and the dominance of crystal-plastic deformation mechanisms in quartz and feldspars in the amphibolite-facies domain (Hirth and Tullis, 1992; Tullis and Yund, 1992; Stipp et al., 2002).

3.4. Clinopyroxenite/hornblende-gabbro composite dikes

Two mappable clinopyroxenite/hornblende-gabbro composite dikes intrude both the metavolcaniclastic and metasedimentary units at Pigeon Point (Fig. 2). These dikes are centered within the domain of L tectonite formation and are associated with the increase in metamorphic temperature outlined above. They consist of cores of coarse-grained to pegmatitic clinopyroxenite rimmed by pegmatitic hornblende gabbro. Contacts between the dikes and their wall rocks are sharp. The long axes of the dikes themselves are parallel with the solid-state deformation fabric in the wall rocks, and they contain a variable linear magmatic fabric that intensifies near the dike margins and is also parallel with the solid-state

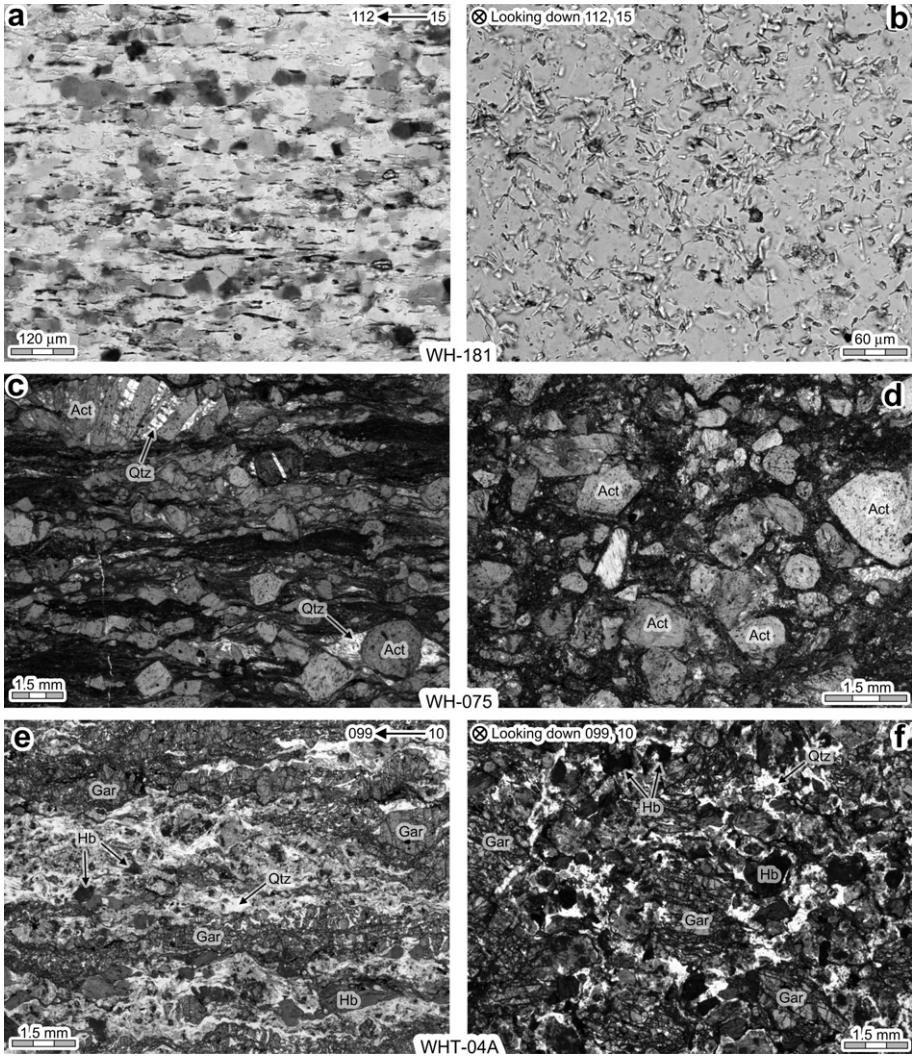

Fig. 4. Photomicrographs of L tectonites from the PPHSZ arranged as lineation-parallel and lineation-perpendicular pairs. (a) Lineation-parallel section of amphibolite-facies meta-argillite. Note the strong alignment of mica grains and the semi-polygonal shape of recrystallized quartz grains. (b) Lineation-perpendicular section of amphibolite-facies meta-argillite. Note the random orientation of high-relief mica grains and the lack of an apparent deformation fabric. (c) Lineation-parallel section of greenschist-facies volcaniclastic breccia. Note the strong alignment of porphyroclasts, pressure-shadow overgrowths, and matrix minerals. (d) Lineation-perpendicular section of greenschist-facies volcaniclastic breccia. Note the random orientation of porphyroclasts and the lack of an apparent deformation fabric. (e) Lineation-parallel section of garnet amphibolite. Note elongate aggregates of fractured garnet grains. (f) Lineation-perpendicular section of garnet amphibolite. Note the lack of an apparent deformation fabric and the fractured nature of garnet grains. (a) Was taken under parallel-polarized light. All others were taken under plane-polarized light. Sample numbers are given at the bottom center of each photo pair. Sample locations are noted in Fig. 2. WH-181 (a, b) and WHT-04A (e, f) are oriented samples and the orientation of the lineation relative to the photographs is given at the top of each pair. WHT-04A was collected by A. W. Snoke. Act = actinolite, Gar = garnet, Hb = hornblende, and Qtz = quartz.

deformation fabric in the wall rocks. Wright and Fahan (1988) interpreted these dikes as synkinematic and obtained hornblende K–Ar ages of 171 ± 1.8 Ma and 169 ± 1.2 Ma from the dikes and 168 ± 3.4 Ma from the adjacent amphibolite.

4. Geometry of the Pigeon Point high-strain zone

4.1. Description of the deformation fabrics

The PPHSZ is marked by a strong, pervasive mineral lineation and a penetrative foliation. In greenschist-facies tectonites of the metavolcaniclastic unit, the mineral lineation is defined by streaking of compositional domains, an alignment of metamorphic minerals (particularly actinolite), and a weak alignment of pseudomorphed phenocrysts and associated pressure-shadow overgrowths (Fig. 4c). The long axes of elongated tuff-breccia clasts are always subparallel with the mineral lineation (Fig. 3b), and slight deviations between clast orientation and mineral-lineation orientation do not occur in any systematic manner. These observations coupled with the observation that there is no evidence for a pre-existing preferred orientation of tuff-breccia clasts outside of the PPHSZ (Fig. 3a) indicates that the mineral lineation defines the principal finite elongation direction. In L–S and $L > S$ tectonites of the metavolcaniclastic unit, foliations are defined by an alignment of metamorphic minerals, flattening of compositional domains, and a weak alignment of pseudomorphed phenocrysts and associated overgrowths. The long axes of tuff-breccia clasts observed on foliation-normal faces are subparallel with the trace of the metamorphic foliation indicating that the pole to the foliation defines the maximum finite shortening direction in these tectonites. In amphibolite-facies tectonites of the metavolcaniclastic unit, the lineation is defined by an alignment of hornblende $\pm$ elongate garnet grains (Fig. 4e). In hand sample, the elongate garnet grains appear to be single crystals. However, under the microscope, garnet

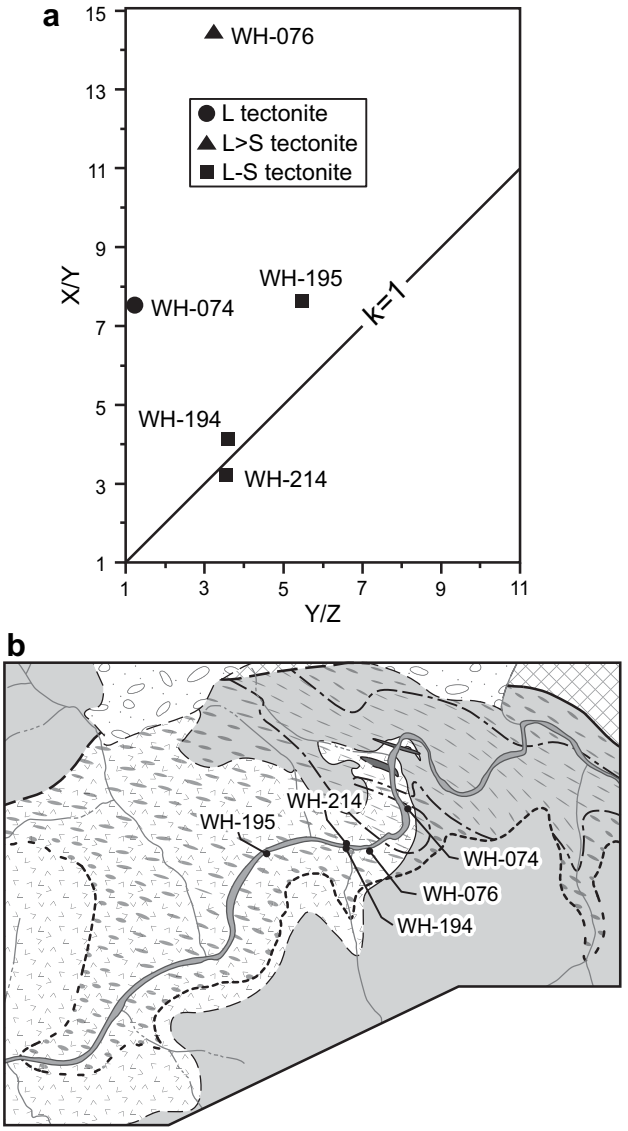

Fig. 5. (a) Flinn diagram showing quantitative finite-strain estimates from the PPHSZ. Estimates were made by measuring elongated tuff-breccia clasts on lineation-perpendicular and lineation-parallel faces. X/Y and Y/Z are the ratios between the long and intermediate and intermediate and short axes of the finite-strain ellipsoid respectively. The line $k = 1$ indicates perfect plane strain. (b) Simplified map of the PPHSZ showing locations of samples in (a). Map symbols are the same as in Fig. 2.

grains appear as aggregates of fractured garnet crystals wherein the fractures are infilled by quartz, carbonate minerals, and minor chlorite (Fig. 4e,f). Quartz infilling fractured garnet grains is generally not dynamically recrystallized, and I interpret fracturing of the garnet as a late-stage deformation feature. Lineations in the metasedimentary unit are defined by a quartz grain-shape alignment, aligned metamorphic minerals, streaking on foliation faces, and, in L tectonites, by pervasively folded and mullioned compositional banding (Fig. 4a). Foliations in these rocks are generally subparallel with the original bedding and are defined by a quartz grain-shape alignment and aligned chlorite, biotite, white mica, and graphite(?) grains.

L tectonites in the PPHSZ display a unique set of microstructural features on lineation-normal faces that also argue in favor of true constrictional deformation. Despite the strong mineral shape fabrics visible on lineation-parallel faces, there is no discernable mineral shape fabric visible on lineation-normal faces of L tectonites of all of the different rock types cut by the PPHSZ (Fig. 4). Porphyroclasts in greenschist-facies L tectonites of the metavolcaniclastic unit show no shape-preferred orientation (Fig. 4d), and they are sometimes completely rimmed by seams of fine-grained epidote, indicating pressure solution took place all the way around the clasts. Amphibole grains are oriented such that basal sections are commonly presented on lineation-normal faces, but their intermediate axes show little or no preferred orientation. In siliceous meta-argillites of the metasedimentary unit, basal cleavage traces of micas are randomly oriented when viewed in lineation-normal sections (Fig. 4b). These rocks also display compositional segregation at the hand-sample scale with quartz-rich domains being completely encircled by micaceous domains. Quartz shows no grain-shape-preferred orientation on lineation-normal faces despite displaying abundant evidence for crystal-plastic deformation.

4.2. Finite-strain estimates

During geologic and structural mapping of this area, I qualitatively estimated the shape of the finite-strain ellipsoid and relative magnitude of finite-strain at each field station. A few of the excellent water-worn exposures along the Trinity River also allow quantitative finite-strain estimates obtained by measuring the axial ratios of elongated tuff-breccia clasts on mutually perpendicular faces. At each locality, clasts were measured on faces normal to both the mineral lineation and foliation and on foliation-parallel faces and/or faces parallel with the lineation and perpendicular to the foliation. Lineation-normal faces yield 20 or more measurements at each locality, whereas lineation-parallel faces typically expose 8–12 measurable clasts. The harmonic mean of all of the axial ratios was calculated for each face. These results are reported in Fig. 5. Localities WH-194 and WH-214 are located on opposite sides of the Trinity River, separated by no more than 40 m (Fig. 2), and I interpret the variation between these two estimates as largely reflecting the error in my quantitative strain analyses (Fig. 5). Qualitative strain estimates fall into three categories; L tectonites, $L > S$ tectonites, and L–S tectonites. For example, locality WH-076, plotted on the Flinn diagram in Fig. 5, lies well into the constrictional field, but a measurable foliation is still apparent in outcrop. Therefore, it is classified as $L > S$ tectonite. Similarly, sample WH-074 (Figs. 3b and 5) has no measurable foliation in outcrop and is classified as an L tectonite. Rocks exposed at localities WH-194, WH-195, and WH-214 (Figs. 2 and 5) are considered L–S tectonites. Qualitative estimates were based on both the relative intensities of foliations and lineations and, where possible, on examinations of tuff-breccia clasts insufficiently exposed for quantitative analyses.

4.3. Internal geometry of the high-strain zone

A one-kilometer-wide, east-southeast-trending domain of well-developed L tectonites in which no foliation can be discerned in outcrop despite a strong, pervasive linear fabric is centered about Pigeon Point within the PPHSZ (Fig. 2). This domain extends along trend throughout the exposed portion of the PPHSZ and includes both the metavolcaniclastic and metasedimentary units. It narrows upwards, and $L > S$ and, locally, L–S tectonites structurally overlie much of the L tectonite domain. A few local domains of $L > S$ tectonites are hosted in the L tectonite domain. Examination of the almost continuous exposures along the Trinity River downstream from Pigeon Point shows that the transition from L tectonites to L–S tectonites takes place over an across-trend horizontal distance of 200–300 m.

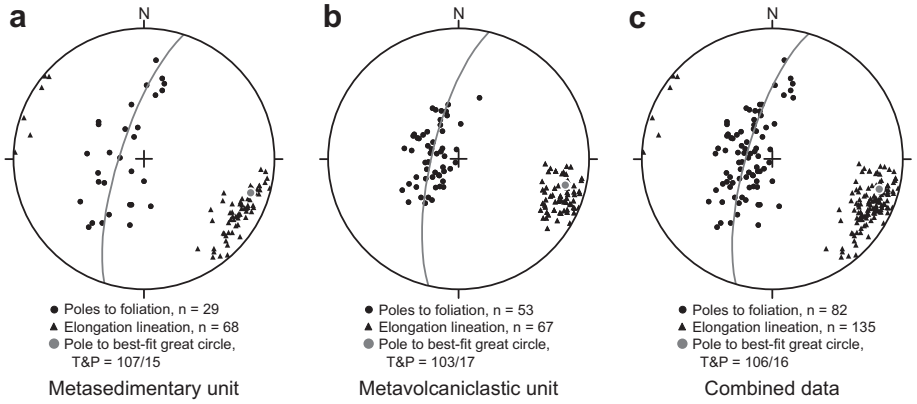

Fig. 6. Orientation of foliation and lineation data from the PPHSZ plotted on equal-area, lower-hemisphere projections. (a) Data from the metasedimentary unit. (b) Data from the metavolcaniclastic unit. (c) Combined data from the metasedimentary and metavolcaniclastic units. Note that the poles to the best-fit great circles to the poles to foliation all lie on the lineation measurements.

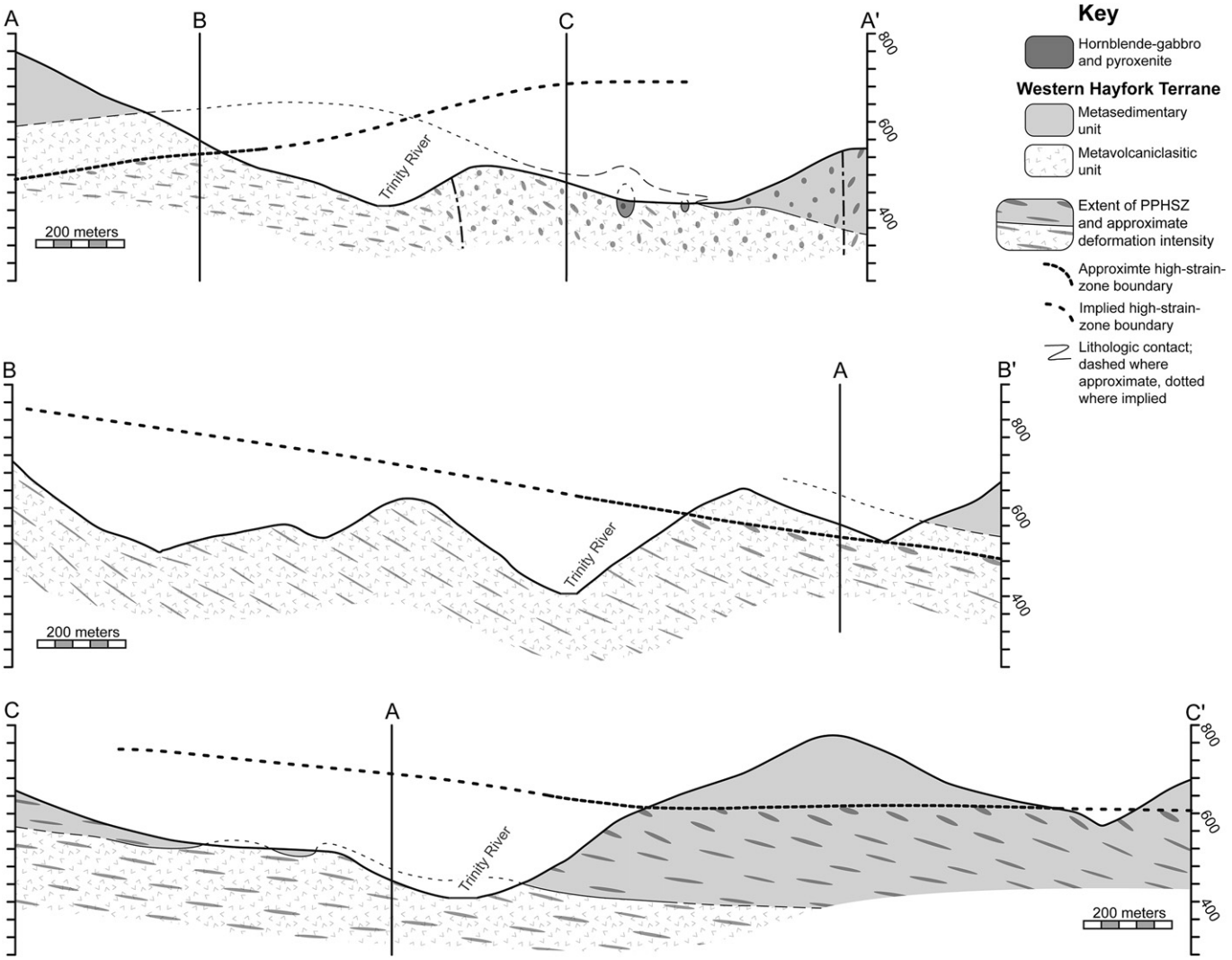

Fig. 7. Cross-section reconstructions of the PPHSZ. A–A′ is a lineation-perpendicular cross-section through the domain of L tectonites. B–B′ is a lineation-parallel cross-section outside of the domain of L tectonites. C–C′ is a lineation-parallel cross-section through the domain of L tectonites. Locations of cross-section lines are displayed in Fig. 2. The pattern of ellipses within the PPHSZ is generalized and intended to show the approximate shape of finite-strain ellipsoids viewed on vertical faces.

Mineral lineations in the PPHSZ plunge gently to the east-southeast to southeast, with the most southerly trends occurring in the southeasterly most part of the domain of L tectonites (Figs. 2 and 6). This systematic spatial change in lineation orientation is reflected in the apparent scatter of lineation orientations in the stereonet plot of fabric elements from the metasedimentary unit (Fig. 6a). Because lineations in L, L > S, and L–S domains in all of the rock types are parallel with one another across lithologic contacts (Fig. 2), this spatial change in lineation orientation is not interpreted as rheologically driven.

At both the northeast and southwest edges of the domain of L tectonites, the strike of foliation in L > S tectonites is close to the trend of the lineation, and foliations on both edges of the L tectonite domain dip moderately to steeply towards the domain of L tectonites (Figs. 2 and 7a). Because of this systematic change in foliation dip approaching the domain of L tectonites, poles to foliation within the PPHSZ loosely define a great-circle distribution centered about the elongation lineations (Fig. 6). This great-circle distribution is more pronounced in the metasedimentary unit (Fig. 6a) because most of the L > S tectonite domains that mantle the L tectonites are in this unit. The systematic change in foliation orientation at the margins of the L tectonite domain could be a result of: (1) active folding of the foliation during progressive deformation, (2) an increasing component of subhorizontal, transport-perpendicular shortening partitioned into this domain, or (3) both of these mechanisms. A lack of thin section- and outcrop-scale evidence for folding of a preexisting foliation, the observation that L > S tectonites transition progressively into L tectonites, and the observation that shape fabrics are parallel with the axes of the finite-strain ellipsoid throughout the PPHSZ indicate that the great-circle distribution of poles to foliation in the PPHSZ is a result of an increasing component of subhorizontal, transport-perpendicular shortening partitioned into the area around the L tectonite domain rather than active folding.

Outside of the domain of L tectonites, the strike of foliation in the PPHSZ varies from northeast–southwest to northwest–southeast, and foliation planes dip gently to the east (Fig. 2). In the area of Logan Gulch, the strike of foliation varies systematically, changing from ~east–west to ~north-northeast–south-southwest and back to ~east–west again (Fig. 2). This systematic change does not occur elsewhere within the resolution of the map data. On the south side of the river, the dip of the foliation is typically oblique to the high-strain-zone boundary by 10° or more (Fig. 2).

In the PPHSZ, the contact between the metasedimentary and metavolcaniclastic units is roughly northwest–southeast-striking and gently northeast-dipping. In the domain of L tectonites at Pigeon Point, the contact between these two units is folded. An open antiform is centered about the larger of the two composite dikes, and a smaller recumbent fold is exposed on the northeast side of Pigeon Point and cut by the smaller of the two composite dikes (Figs. 2 and 7a). Orientations of map-scale fold hinge lines cannot be precisely determined, but they are generally subparallel with mineral lineations in the L tectonite domain. These folds further indicate that the domain of L tectonites records localized high-strain-zone-parallel, lineation-perpendicular shortening.

4.4. External geometry of the high-strain zone

I mapped the upper boundary of the PPHSZ along the steep sides of the Trinity River valley as accurately as possible using traditional geologic mapping methods and a GPS unit (Fig. 2). A thorough examination of the nearly continuous exposures along the hogback ridge above Pigeon Point on the south side of the river unequivocally demonstrates that the deformation fabric in the PPHSZ progressively weakens upwards from the river level to the high-strain-zone boundary. The boundary of the high-strain zone is located where deformation fabrics are indistinguishable from the regionally developed weak foliation. Throughout the area, the upper high-strain-zone boundary lies at least 300 m structurally below the position of the Wilson Point thrust mapped by Fahan

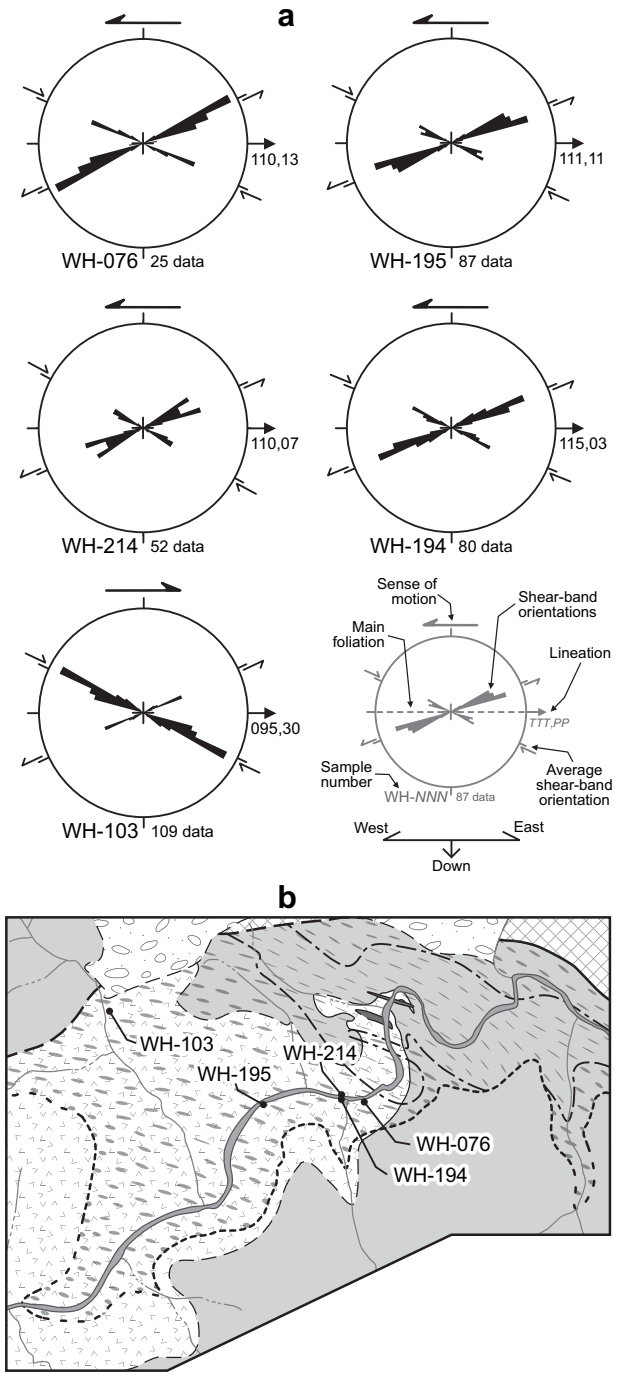

Fig. 8. (a) Shear-band orientations from the domain of L – S and L > S tectonites within the PPHSZ. Rose diagrams are viewed to the north as near-vertical sections—perpendicular to the foliation and parallel with the mineral lineation. Plots contain every shear band found in a standard thin section. Data are plotted by class frequency, and the outer circle represents 30% of the total data points. Four-out-of-five samples indicate top-to-the-west, reverse-sense displacement. One sample (WH-103) indicates top-to-the-east, normal-sense displacement. Conjugate sets of shear bands are present in all of the samples. Maximum shear-band inclinations are given in Table 1. Orientations of mineral lineations are noted. (b) Simplified map of the PPHSZ showing locations of samples in (a). Map symbols are the same as in Fig. 2.

(1982), and the lower boundary is not exposed. Across- and along-trend projections of the high-strain-zone boundary along lines A–A′, B–B′, and C–C′ are presented in Fig. 7. The orientation of the high-strain-zone boundary in these sections is constrained by: (1) the mapped position of the boundary, (2) three-point-problem solutions conducted where the boundary is cut by tributary valleys, and (3) the observation that rocks in float on top of the unnamed knoll between lines B–B′ and C–C′ on the north side of the river contain a strong L–S deformation fabric indicating that the high-strain-zone boundary must project well above the ~800-m elevation of this point (Fig. 2). In the domain of L–S tectonites, in the west half of the exposed part of the PPHSZ, the high-strain-zone boundary is roughly east–west-striking and gently south-dipping (Figs. 2 and 7a,b). Moving across-trend towards the northeast into the domain of L tectonites, the high-strain boundary is interpreted to warp upwards (Figs. 2 and 7a). Above the domain of L tectonites, along line C–C′, the high-strain-zone boundary is subhorizontal to northeast–southwest-striking and gently southeast-dipping (Figs. 2 and 7c), and I interpret this area as being at the culmination of a convex-upwards warp of the high-strain-zone boundary.

5. Kinematic analyses

5.1. Sense of shear

During geologic and structural mapping, oriented samples were collected for thin section-based kinematic analyses. Samples were cut perpendicular to and parallel with the three principal elongation directions defined by the foliation and the mineral lineation. Thin sections were predominately prepared from lineation-parallel cuts in samples of both L and L–S tectonites. Thin sections from lineation-perpendicular and foliation-parallel cuts were also prepared from several samples. Deformation fabrics viewed on both lineation-parallel and lineation-perpendicular faces are highly symmetrical. However, conjugate sets of weakly developed shear bands (Berthé et al., 1979; Platt and Vissers, 1980) and local asymmetric pressure-shadow overgrowths on porphyroclasts (Etchecopar and Malavieille, 1987) are visible in thin sections cut from faces perpendicular to the foliation and parallel with the lineation in L–S and L > S tectonites collected from the metavolcaniclastic unit. The dominate orientation of shear bands from four out of five of these samples indicates top-to-the-west, reverse-sense displacement, and the other sample indicates top-to-the-east, normal-sense displacement (Fig. 8). Top-to-the-west, reverse-sense displacement is also indicated by the sense of obliquity between foliations and the high-strain-zone boundary, with foliations just beneath the boundary dipping $\geq 10^\circ$ more steeply to the east (Figs. 2 and 7b).

5.2. Kinematic-vorticity estimates

The highly symmetrical character of the deformation fabrics and the presence of conjugate sets of shear bands visible on faces viewed perpendicular to the foliation and parallel with the lineation indicates that L − S and L > S tectonites within the PPHSZ record a significant component of coaxial deformation that accommodated foliation-normal contraction and transport-parallel elongation and extrusion of material out of the zone (Platt and Vissers, 1980). A useful measure of the degree of noncoaxiality of flow is the kinematic-vorticity number (W_k) (Truesdell, 1954; see also reviews by Means et al., 1980; Simpson and De Paor, 1993; Tikoff and Fossen, 1995). For the simple case of two-dimensional deformation with no net external rotation, W_k can be defined as the cosine of the acute angle between the flow apophyses or the flow eigenvectors (Means et al., 1980; Simpson and De Paor, 1993). In such case, W_k will range from zero (cosine 90°) for coaxial deformation to one (cosine 0°) for the case of strict simple shear. The intermediate case, or roughly equal contributions of pure shear and simple shear, occurs at $W_k = 0.71$ (cosine 45°).

Simpson and De Paor (1993) tentatively proposed that synthetic and antithetic shear bands will nucleate parallel with the acute and obtuse bisectors of the stable flow eigenvectors respectively during steady-state, monoclinic, general-shear deformation. Kurz and Northrup (2008) tested this hypothesis using naturally deformed rocks and concluded that synthetic and antithetic shear bands initially nucleate parallel with the acute and obtuse bisectors of the stable flow eigenvectors and progressively rotate towards parallelism with the flow plane of the simple-shear component of flow as deformation proceeds. With this relationship W_k can be estimated using the equation

$$W_k = \cos(2\alpha)$$

where α is the greatest angle between a synthetic shear band and the flow plane of the simple-shear component of deformation, one of the stable eigenvectors (Kurz and Northrup, 2008). The α values and their corresponding W_k estimate from the PPHSZ samples are listed in Table 1. Maximum angles between antithetic shear bands and the flow plane in these samples are not large enough to define the obtuse bisector between the stable flow eigenvectors (Table 1). However, the sample sets of antithetic shear bands are small, and they are even more poorly developed than the synthetic shear bands. For these reasons, I may have failed to find or recognize antithetic shear bands at or near their initial nucleation orientation. The orientation of the flow plane of the simple-shear component of deformation was approximated as the orientation of the foliation. For relatively low finite strains and/or simple-shear-dominated deformation this should lead to underestimates of the angle between the stable eigenvectors and hence W_k. However, samples used in these analyses appear to record pure-shear-dominated deformation and relatively large finite strains, and the foliation is generally subparallel with the long axis of the finite-strain ellipsoid. Therefore, it is reasonable to assume that the foliation is subparallel with the flow plane of the simple-shear component and hence one of the stable flow eigenvectors. Because shear bands are assumed to rotate away from the acute bisector of the stable flow eigenvectors after initial nucleation, this method for estimating W_k provides a maximum possible value of the simple-shear component of deformation in these samples, as it is unlikely that my relatively small data sets sample a shear band at the initial stages of formation. Also, this method utilizes data collected on two-dimensional section planes and is not strictly valid for non-plane-strain deformation. However, Tikoff and Fossen (1995, pp. 1776–1777) have shown that two-dimensional kinematic-vorticity analyses of three-dimensional, monoclinic deformations will consistently overestimate W_k by only a small amount. Overestimation will be greatest for nearly equal components of coaxial and noncoaxial deformation and will decline to zero as W_k goes to zero or one. For

Table 1
Angles between shear bands and the main foliation and corresponding values of kinematic vorticity.

Sample	Apparent sense of motion	Greatest inclination of synthetic shear bands (α)	W_k	% simple shear	Greatest inclination of antithetic shear bands
WH-076	Reverse	33°, $n = 17$	0.41	27%	33°, $n = 08$
WH-103	Normal	42°, $n = 83$	0.10	7%	37°, $n = 26$
WH-194	Reverse	32°, $n = 54$	0.44	29%	39°, $n = 26$
WH-195	Reverse	37°, $n = 60$	0.28	18%	37°, $n = 27$
WH-214	Reverse	40°, $n = 35$	0.17	11%	41°, $n = 17$

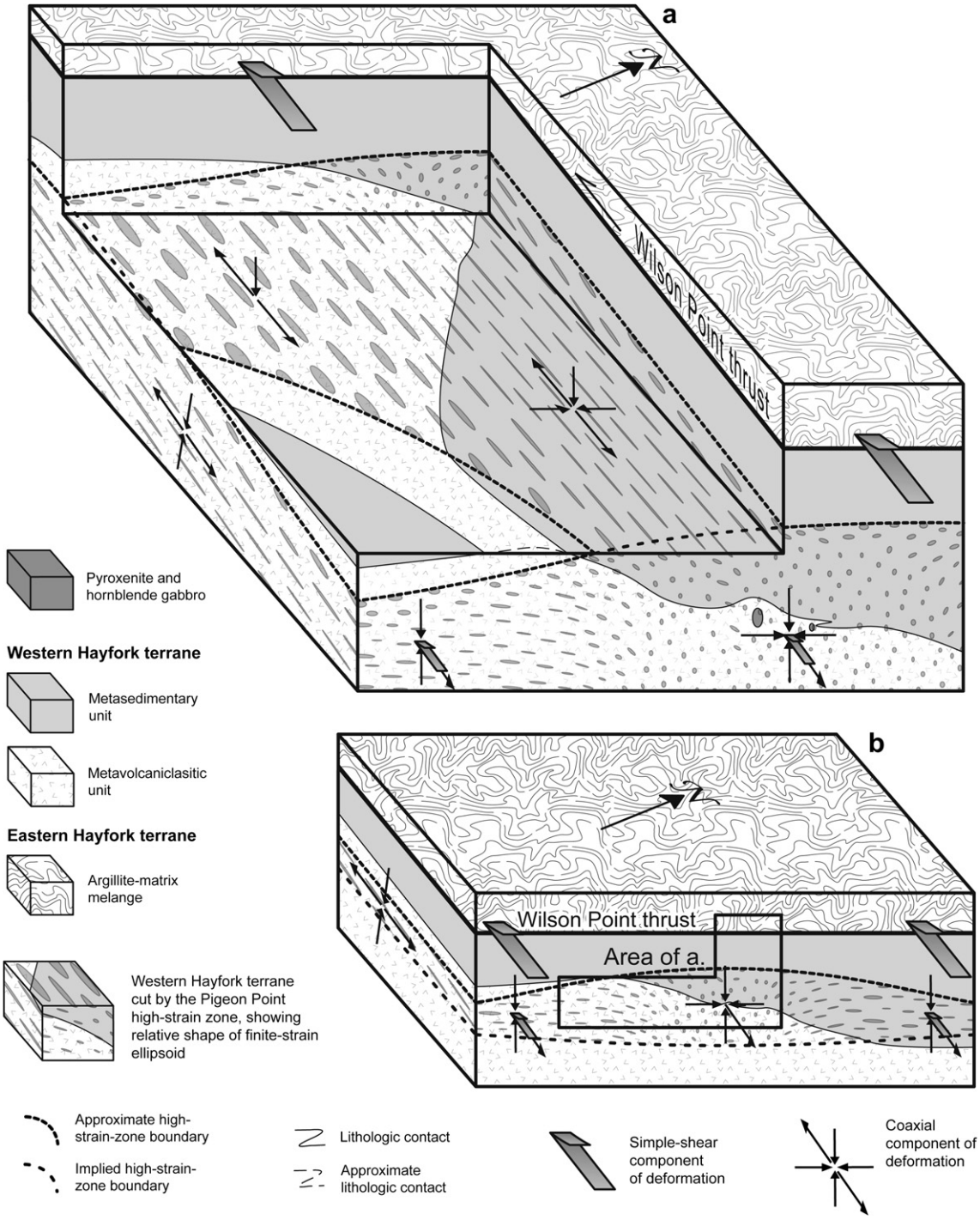

Fig. 9. (a) Block-diagram cartoon showing the three-dimensional geometry of the PPHSZ developed from the map data, cross-section reconstructions, and kinematic data. (b) Block-diagram cartoon showing the inferred convex-upwards, lens-shaped geometry of the PPHSZ. The domain of L tectonites lies in a narrow corridor in the center of the PPHSZ and accommodates a component of subhorizontal, strike-parallel flow in addition to the component of subhorizontal, strike-perpendicular flow accommodated throughout the zone.

microstructural approaches to estimating W_k, overestimation due to non-plane-strain deformation is probably less than the measurement error. Finally, these estimates are based on fabric elements that only record the last increments of deformation and therefore may not be true estimates of the mean vorticity of deformation.

Synthetic shear bands in L–S and L > S tectonites of the PPHSZ suggest W_k values between 0.10 and 0.44 corresponding to simple-shear components of 7–29% (Table 1). Given the large number of uncertainties and assumptions used in obtaining these W_k estimates, they are probably not accurate values of the mean vorticity of flow. However, these estimates combined with the observation that deformation fabrics in the PPHSZ samples are highly symmetrical indicate that flow in L–S and L > S tectonites in the PPHSZ can be broadly characterized as pure-shear dominated. Kinematic-vorticity analyses of L tectonites are problematic because there is no visible foliation to serve as a reference frame for the orientation of the simple-shear component of deformation, and I have not attempted to quantify W_k in these rocks. However, deformation fabrics in all of the lineation-parallel and lineation-

perpendicular thin sections cut from L tectonite samples are also all highly symmetrical regardless of section orientation, and I also interpret the L tectonites as recording pure-shear-dominated deformation.

6. Causes of L tectonite formation

6.1. Summary of important data and observations

The map data and cross-section reconstructions presented above demonstrate that the exposed part of the PPHSZ is an east–west-striking, subhorizontal to gently south-dipping high-strain zone that cuts rocks of the western Hayfork terrane. L–S and L > S tectonites characterize the western half of the exposed part of the PPHSZ, whereas the eastern half of the high-strain zone contains a one-kilometer-wide (across-trend) domain of L tectonites in which no mesoscopic foliation is visible. The domain of L tectonites is associated with: (1) an across-trend convex-upward warp of the upper high-strain-zone boundary, (2) a lithogical and hence rheological transition from mafic metavolcaniclastic rocks to micaceous quartzites and quartzose schists, (3) folding of this rheological boundary, (4) the emplacement of synkinematic mafic/ultramafic dikes, and (5) an associated local increase in deformation temperatures in both of the rheologic units from greenschist- to amphibolite-facies conditions creating additional rheologic domains. Finite-strain and microstructural analyses of L tectonites show that these rocks record nearly pure constrictional strain. Microstructural analyses of L − S and L > S tectonites in the western half of the PPHSZ show that the zone records pure-shear-dominated deformation that accommodates zone-normal shortening and transport-parallel elongation coupled with a subordinate component of top-to-the-west-directed simple-shear.

All of these observations and constraints are incorporated into the cartoon block diagram presented in Fig. 9a. In this model, the PPHSZ is confined to the western Hayfork terrane and records zone-normal shortening and transport-parallel extrusion of material out of the deformation zone. At the same time, top-to-the-west, reverse-sense displacement between the western Hayfork terrane and the structurally overlying eastern Hayfork terrane is almost entirely partitioned into the Wilson Point thrust zone.

6.2. Kinematic significance of L tectonites

The domain of L tectonites localized a significant component of constrictional pure shear resulting from zone-parallel, transport-perpendicular flow. L tectonites are localized in a narrow corridor in the convex-upwards, high-strain zone that is flanked on at least one side by a large domain of L–S and L > S tectonites. Based on these observations, I propose that the PPHSZ is a lens-shaped zone with domains of L–S and L > S tectonites originally flanking the domain of L tectonites on either side (Fig. 9b). Lateral flow into the domain of L tectonites resulting from zone-normal contraction requires either strain in the flattening field outside the domain of L tectonites or bulk constrictional strain across the PPHSZ. Significant flattening strains are not recorded in the exposed part of the high-strain zone, but they may exist in unexposed parts of the zone, so neither of these possibilities can be ruled out. Although, bulk strain in the constrictional field is more likely. This geometry requires a triclinic deformation symmetry in at least part of the PPHSZ to accommodate simultaneous strike-parallel, lineation-perpendicular flow into the domain of L tectonites and the component of top-to-the-west, reverse-sense motion. Although, I found no evidence of a triclinic deformation geometry in my microstructural analyses of lineation-perpendicular sections. This could be because the deformation is only slightly triclinic. Alternatively, the strike-parallel, lineation-perpendicular simple-shear component of deformation may have been localized near the high-strain-zone boundary where unweathered exposures are scarce and I was not able to collect fresh samples. In either case, the large apparent inclinations of synthetic shear bands indicates that lineation-parallel thin sections used in the kinematic analyses are close to perpendicular to the vorticity vector.

Flinn (1961) used an unscaled analogue model to investigate formation of constrictional strain in rectangular grooves in one boundary of a high-strain zone undergoing zone-normal contraction and found that flow within the groove and hence the development of constrictional strain will not initiate until the groove depth exceeds the thickness of the high-strain zone outside of the groove. In the PPHSZ, the convex-upwards warp of the high-strain-zone boundary over the domain of L tectonites does not provide sufficient relief to meet this criterion. However, Flinn's (1961) model recorded bulk strain in the flattening field because it was not constrained laterally. Bulk plane-strain or constrictional deformation would certainly favor flow into the existing channel in the high-strain-zone boundary and the formation of L tectonites. Also, the geometry of the lower boundary of the PPHSZ is completely unconstrained. If the lower boundary of the zone mirrors the upper boundary, this would effectively produce a deeper channel, also favoring flow into this domain and the formation of L tectonites. Therefore, I propose that localization of the domain of L tectonites is at least in part a function of the convex-upward warp of the high-strain-zone boundary favoring zone-parallel, strike-perpendicular flow into this domain.

There are no obvious lithological transitions controlling the orientation and location of the boundaries of the PPHSZ. Hence, the convex-upward warp of the high-strain-zone boundary was probably caused by: (1) a local increase in deformation temperature and possibly metamorphic fluids associated with the composite dikes centered within the domain of L tectonites, and/or (2) local variations in the boundary conditions that drove the formation of the PPHSZ in the first place. About three kilometers west-southwest of the PPHSZ, a similar high-strain zone cuts exposures of the metavolcaniclastic unit that crop out along the Trinity River just upstream of the town of Big Flat. This structure has not been named in the literature, so I will hereon refer to it as the Big Flat high-strain zone. The Big Flat high-strain zone is characterized by east-trending, moderately plunging elongation lineations; east–west- to northeast–southwest-striking, moderately dipping foliations; and plane strain or strain in the constrictional field. At least one outcrop-scale domain of L tectonites is also present. A >200-m-wide clinopyroxenite/hornblende-gabbro body intrudes the westernmost exposed part of the Big Flat high-strain zone, and this body caused a local increase in metamorphic temperatures from greenschist- to amphibolite-facies conditions. Greenschist-facies deformation fabrics in the Big Flat high-strain zone can be traced continuously into amphibolite-facies fabrics, and the two domains exhibit similar fabric orientations. Based on these relationships, I interpret the composite intrusive body as syntectonic. Because deformation in both the PPHSZ and Big Flat high-strain zone is directly related to the local intrusive bodies, and there are no intrusive bodies in the weakly deformed rocks between the two high-strain zones, I propose that local temperature increases and perhaps local increases in metamorphic fluids played a direct role in initiating intense plastic deformation in these zones. This proposal favors the hypothesis that the convex-upwards shape of the high-strain-zone boundary above the domain of L tectonites in the PPHSZ was caused by the localization of magmatic heat in this domain. At the same time, zone-normal contraction and localized transport-perpendicular, strike-parallel flow into the domain of L

tectonites are still required to produce local constrictional strain, making the formation of L tectonites within the PPHSZ a function of both a local variation in the shape of the high-strain-zone boundary driven by magmatic heating, and a kinematic geometry favorable for the localization of constrictional strain in this domain. L tectonites within the PPHSZ are developed in both the metasedimentary and metavolcaniclastic units deformed under greenschist- and amphibolite-facies conditions, and deformation-fabric elements in all of these rheologic units are parallel with each other at lithologic contacts. Hence, constrictional strain is not being partitioned into a single rheological domain.

6.3. Incorporation into the regional geologic framework

Direct constraints on the timing of deformation in the PPHSZ are provided by hornblende K–Ar cooling ages of 169 ± 1.2 and 171 ± 1.8 Ma from the syntectonic composite dikes exposed at Pigeon Point and a hornblende K–Ar cooling age of 168 ± 3.4 Ma from the amphibolite associated with these dikes (Wright and Fahan, 1988). The existence of metamorphic minerals and deformation textures consistent with amphibolite-facies conditions indicates that deformation in the PPHSZ was at least in part coeval with local amphibolite-facies metamorphism associated with these dikes. Based on the local syntectonic replacement of hornblende by actinolite in amphibolites and relatively low-temperature subgrain-rotation dynamic recrystallization (regime-II–III transition of Hirth and Tullis, 1992) of quartz, I infer that deformation continued for a short time after cooling through the Ar closure temperature of hornblende. These observations place the PPHSZ in a well-established Middle Jurassic episode of thrust faulting, regional metamorphism, and penetrative fabric development: the Siskiyou event outlined above. Two possibilities then exist for the structural significance of the PPHSZ: (1) it may be the hanging-wall exposure of a large-displacement plastic thrust zone separating two terranes (e.g. the Salt Creek fault that separates the western Hayfork terrane from the underlying Rattlesnake Creek terrane; Wright and Fahan, 1988) or (2) it may be an intra-terrane structure related to contractional deformation and terrane amalgamation, but not a major terrane boundary. Because deformation in the PPHSZ was pure-shear dominated, the first possibility can be eliminated. Instead, the PPHSZ accommodated a limited amount of top-to-the-west, reverse-sense displacement and a significant amount of subvertical shortening and extrusion of material out of the deformation zone. This geometry developed in response to contractional deformation and thrust loading associated with terrane amalgamation during the Middle Jurassic Siskiyou event and is temporally related to the overlying west-vergent Wilson Point thrust which is cut by the ~170-Ma Ironside Mountain batholith (Barnes et al., 2006). Therefore, the coeval PPHSZ/Wilson Point-thrust system represents deformation-path partitioning during assembly of the western Hayfork and eastern Hayfork terranes. In this system simple-shear deformation accommodating large-magnitude, reverse-sense displacement between the two tectonically distinct telescoped crustal fragments was partitioned into the Wilson Point thrust zone. I was unable to locate exposures of the Wilson Point thrust zone during regional reconnaissance, and the exact nature of this fault zone is not described in the literature. Therefore, I can only speculate about the mechanisms (frictional/brittle faulting vs. plastic flow) that accommodated simple-shear translation between the western Hayfork and eastern Hayfork terranes. At the same time slip across the Wilson point thrust was occurring, plastic, pure-shear-dominated deformation in the PPHSZ (and probably the Big Flat high-strain zone as well) helped to accommodate crustal thickening during terrane amalgamation through subhorizontal shortening coupled with extrusion of material from beneath the structurally overlying Wilson Point thrust and eastern Hayfork terrane towards the orogenic front to the west. Thus, the PPHSZ represents a mid-crustal mechanism for accommodating variable crustal thickening during terrane amalgamation and continental assembly by plastic flow from beneath a major thrust plate catalyzed by local magmatic heating.

7. Summary and conclusions

Detailed geologic mapping, strain analyses, and kinematic analyses, enable the reconstruction of a one-kilometer-wide domain of L tectonites within the gently dipping PPHSZ in the southern Klamath Mountains, California. The domain of L tectonites is associated with: (1) an across-trend, convex-upward warp of the upper high-strain-zone boundary, (2) a lithologic and hence rheological transition from mafic metavolcaniclastic rocks to micaceous quartzites and quartzose schists, (3) folding of this rheological boundary, (4) the emplacement of synkinematic ultramafic/mafic intrusive bodies, and (5) an associated local increase in metamorphic temperature in both of the rock units from greenschist- to amphibolite-facies conditions creating additional rheologic domains. Microstructural analyses of L–S and $L > S$ tectonites in the western half of the PPHSZ indicate pure-shear-dominated deformation that accommodated zone-normal shortening and transport-parallel elongation coupled with a subordinate component of top-to-the-west-directed simple shear. The localization of constrictional strain in the L tectonite domain was likely controlled by the shape of the high-strain-zone boundary causing lateral flow into the apex of the lens-shaped zone in response to a favorable kinematic geometry that includes zone-normal shortening coupled with transport-parallel elongation and probably bulk strain in the constrictional field throughout the zone. Localized magmatic heating is the best explanation for the shape of the high-strain-zone boundary. Localization of constrictional strain does not seem to be related to the rheological and metamorphic transitions within the PPHSZ because the domain of L tectonites cuts all of the rheologic units and deformation-fabric elements in all of the units are parallel with one another across lithologic contacts. This structural geometry developed in response to regional contractional deformation, terrane amalgamation, and thrust loading during a Middle Jurassic orogenic event and helped to accommodate crustal thickening during terrane accretion and continental growth along a subduction margin. The coeval PPHSZ/Wilson Point-thrust system records deformation-path partitioning between localized top-to-the-west simple-shear along the Wilson Point thrust and distributed subvertical shortening and transport-parallel elongation in the underlying plastic PPHSZ. Terrane assembly was accomplished by simple shear deformation along the Wilson Point thrust while the plastic PPHSZ accommodated crustal thickening by moving material back towards the orogenic front.

Acknowledgements

Funding for this study was provided by the Gregg Ranch Foundation and the University of Wyoming Department of Geology and Geophysics. The program *Stereonet* created by R. Allmendinger was used to plot the orientation data. A. W. Snoke is thanked for introducing me to the area, providing reconnaissance samples, and spending time with me in the field. S.R. Garlick and E. Kingsbury helped collect quantitative finite-strain data, and Trinity River Rafting provided a boat and two guides for a day. I completed much of this work while in residence at the University of Wyoming, and B.R. Frost, S.T. Jackson, B.E. John, R.D. Law, and A.W. Snoke provided helpful comments while serving on my Ph.D. examining committee. The manuscript was further improved by reviews from

M. Swanson and editor J. Hippertt, but any remaining errors of omission or interpretation are my own.

References

Allen, C.M., Barnes, C.G., 2006. Ages and some cryptic sources of Mesozoic plutonic rocks in the Klamath Mountains, California and Oregon. In: Snoke, A.W., Barnes, C.G. (Eds.), Geological Studies in the Klamath Mountains Province, California and Oregon. Geological Society of America Special Paper, vol. 410, pp. 223–245.

Ando, C.J., Irwin, W.P., Jones, D.L., Saleeby, J.B., 1983. The ophiolitic North Fork terrane in the Salmon River region, central Klamath Mountains, California. Geological Society of America Bulletin 94, 236–252.

Bailey, C.M., Eyster, E.L., 2003. General shear deformation in the Pinaleno Mountains metamorphic core complex, Arizona. Journal of Structural Geology 25, 1883–1892.

Bailey, C.M., Francis, B.E., Fahrney, E.E., 2004. Strain and vorticity analysis of transpressional high-strain zones from the Virginia Piedmont, USA. In: Alsop, G.I., Holdsworth, R.E., McCaffrey, K.J.W., Hand, M. (Eds.), Flow Processes in Faults and Shear Zones. Geological Society, London, Special Publications, vol. 224, pp. 249–264.

Barrow, W., Metcalf, R., 2006. A reevaluation of the paleotectonic significance of the Paleozoic Central Metamorphic terrane, eastern Klamath Mountains: new constraints from trace element geochemistry and $^{40}Ar/^{39}Ar$ thermochronology. In: Snoke, A.W., Barnes, C.G. (Eds.), Geological Studies in the Klamath Mountains Province, California and Oregon. Geological Society of America Special Paper, vol. 410, pp. 393–410.

Barnes, C.G., Mars, E.V., Swapp, S., Frost, C.D., 2006. Petrology and geochemistry of the Middle Jurassic Ironside Mountain batholith: evolution of potassic magmas in a primitive arc setting. In: Snoke, A.W., Barnes, C.G. (Eds.), Geological Studies in the Klamath Mountains Province, California and Oregon. Geological Society of America Special Paper, vol. 410, pp. 199–221.

Berthé, D., Choukroune, P., Gapais, D., 1979. Orthogneiss mylonite and non-coaxial deformation of granites: the example of the South Armorican shear zone. Journal of Structural Geology 1, 31–42.

Brown, E.H., Talbot, J.L., 1989. Orogen-parallel extension in the North Cascades crystalline core. Tectonics 8, 1105–1114.

Coleman, R.G., Manning, C.E., Mortimer, N., Donato, M.M., Hill, L.B., 1988. Tectonic and regional metamorphic framework of the Klamath Mountains and adjacent Coast Ranges, California and Oregon. In: Ernst, W.G. (Ed.), Metamorphism and Crustal Evolution of the Western United States – Rubey Volume VII. Prentice Hall, Englewood Cliffs, New Jersey, pp. 1059–1097.

Condie, K.C., 1982. Plate-tectonics model for Proterozoic continental accretion in the southwestern United States. Geology 10, 37–42.

Czeck, D.M., Hudleston, P.J., 2003. Testing models for obliquely plunging lineations in transpression: a natural example and theoretical discussion. Journal of Structural Geology 25, 959–982.

Davis, G.A., 1968. Westward thrust faulting in the south-central Klamath Mountains, California. Geological Society of America Bulletin 79, 911–934.

Davis, G.A., Holdaway, M.J., Lipman, P.W., Romey, W.D., 1965. Structure, metamorphism, and plutonism in the south-central Klamath Mountains, California. Geological Society of America Bulletin 76, 933–966.

Dickinson, W.R., 2008. Accretionary Mesozic–Cenozoic expansion of the Cordilleran continental margin in California and adjacent Oregon. Geosphere 4, 329–353.

Donato, M.M., 1987. Evolution of an ophiolitic tectonic mélange, northern California Klamath Mountains, USA. Geological Society of America Bulletin 98, 448–464.

Donato, M.M., Barnes, C.G., Tomlinson, S.L., 1996. The enigmatic Applegate Group of southwestern Oregon: age, correlation, and tectonic affinity. Oregon Geology 58, 79–91.

Ernst, W.G., 1999. Mesozoic petrotectonic development of the Sawyers Bar suprasubduction zone arc, central Klamath Mountains, northern California. Geological Society of America Bulletin 111, 1217–1232.

Ernst, W.G., Hacker, B.R., Barton, M.D., Sen, G., 1991. Igneous petrogenesis of magnesian metavolcanic rocks from the central Klamath Mountains, northern California. Geological Society of America Bulletin 103, 56–72.

Etchecopar, A., Malavieille, J., 1987. Computer models of pressure shadows: a method for strain measurement and shear sense determination. Journal of Structural Geology 9, 667–678.

Fahan, M.R., 1982. Geology and geochronology of part of the Hayfork terrane, Klamath Mountains, northern California. M.S. thesis, University of California, Berkley.

Flinn, D., 1961. On deformation at thrust planes in Shetland and the Jotunheim area of Norway. Geological Magazine 98, 245–256.

Flinn, D., 1965. On the symmetry principle and the deformation ellipsoid. Geological Magazine 102, 36–45.

Flinn, D., 1992. Comment on "Ophiolitic mylonites in the Lizard complex: ductile extension in the lower oceanic crust". Geology 19, 954.

Frost, C.D., Fruchey, B.L., Chamberlain, K.R., Frost, B.R., 2006. Archean crustal growth by lateral accretion of juvenile supracrustal belts in the south-central Wyoming Province. Canadian Journal of Earth Sciences 43, 1533–1555.

Garcia, M.O., 1979. Petrology of the Rogue and Galice Formations, Klamath Mountains, Oregon: identification of a Jurassic island arc sequence. Journal of Geology 86, 29–41.

Gerbi, C., West Jr., D.P., 2007. Use of U-Pb geochronology to identify successive, spatially overlapping tectonic episodes during Silurian-Devonian orogenesis in south-central Maine, USA. Geological Society of America Bulletin 119, 1218–1231.

Giorgis, S., Tikoff, B., 2004. Constraints on kinematics and strain from feldspar porphyroclast populations. In: Alsop, I., Holdsworth, R. (Eds.), Transport and Flow Processes in Shear Zones. Geological Society, London, Special Publication, vol. 224, pp. 265–285.

Goodge, J.W., 1989a. Evolving early Mesozoic convergent margin deformation, central Klamath Mountains, northern California. Tectonics 8, 845–864.

Goodge, J.W., 1989b. Polyphase metamorphic evolution of a Late Triassic subduction complex, Klamath Mountains, northern California. American Journal of Science 289, 874–943.

Goodwin, L.B., Williams, P.F., 1996. Deformation path partitioning within a transpressive shear zone, Marble Cove, Newfoundland. Journal of Structural Geology 18, 975–990.

Hacker, B.R., Donato, M.M., Barnes, C.G., McWilliams, M.O., Ernst, W.G., 1995. Timescales of orogeny: Jurassic construction of the Klamath Mountains. Tectonics 14, 677–703.

Hacker, B.R., Mosenfelder, J.L., 1996. Metamorphism and deformation along the emplacement thrust of the Samail ophiolite, Oman. Earth and Planetary Science Letters 144, 435–451.

Harper, G.D., 1984. The Josephine ophiolite. Geological Society of America Bulletin 95, 1009–1026.

Harper, G.D., Grady, K., Wakabayashi, J., 1990. A structural study of a metamorphic sole beneath the Josephine ophiolite, western Klamath terrane, California–Oregon. In: Harwood, D.S., Miller, M.M. (Eds.), Paleozoic and Early Mesozoic Paleogeographic Relations: Sierra Nevada, Klamath Mountains, and Related Terranes. Geological Society of America Special Paper, vol. 255, pp. 379–396.

Harper, G.D., Saleeby, J.B., Heizler, M., 1994. Formation and emplacement of the Josephine ophiolite and the Nevadan orogeny in the Klamath Mountains, California–Oregon: U/Pb zircon and $^{40}Ar/^{39}Ar$ geochronology. Journal of Geophysical Research 99, 4293–4321.

Hill, L.B., 1985. Metamorphic, deformational, and temporal constraints on terrane assembly, northern Klamath Mountains, California. In: Howell, D.G. (Ed.), Tectonostratigraphic Terranes of the Circum-Pacific Region. Circum-Pacific Council for Energy Resources Earth Sciences Series, vol. 1, pp. 173–186.

Hirth, G., Tullis, J., 1992. Dislocation creep regimes in quartz aggregates. Journal of Structural Geology 14, 145–160.

Hotz, P.E., Lanphere, M.A., Swanson, D.A., 1977. Triassic blueschist from northern California and north-central Oregon. Geology 5, 659–663.

Huang, C.Y., Yuan, P.B., Lin, C.W., Wang, T.K., Chang, C.P., 2000. Geodynamic processes of Taiwan arc–continent collision and comparison with analogs in Timor, Papua New Guinea, Urals and Corsica. Tectonophysics 325, 1–21.

Irwin, W.P., 1960. Geologic reconnaissance of the northern Coast Ranges and Klamath Mountains, California, with a summary of mineral resources. California Division of Mines Bulletin 179, 80.

Irwin, W.P., 1972. Terranes of the western Paleozoic and Triassic belt in the southern Klamath Mountains, California. U.S. Geological Survey Professional Paper 800-C, C103–C111.

Irwin, W.P., 1981. Tectonic accretion of the Klamath Mountains. In: Ernst, W.G. (Ed.), The Geotectonic Development of California – Ruby Volume I. Prentice Hall, Englewood Cliffs, New Jersey, pp. 29–70.

Irwin, W.P., 1994. Geologic map of the Klamath Mountains, California and Oregon. U.S. Geological Survey Miscellaneous Investigations Series Map I-2148, scale 1: 500,000.

Irwin, W.P., Jones, D.L., Pessagno Jr., E.A., 1977. Significance of Mesozoic radiolarians from the pre-Nevadan rocks of the southern Klamath Mountains, California. Geology 5, 557–562.

Jessup, M.J., Law, R.D., Searle, M.P., Hubbard, M.S., 2006. Structural evolution and vorticity of flow during extrusion and exhumation of the Greater Himalayan Slab, Mount Everest Massif, Tibet/Nepal: implications for orogen-scale flow partitioning. In: Law, R.D., Searle, M.P., Godin, L. (Eds.), Channel Flow, Extrusion, and Exhumation in Continental Collision Zones. Geological Society, London, Special Publications, vol. 268, pp. 379–414.

Kurz, G.A., Northrup, C.J., 2008. Structural analysis of mylonitic fault rocks in the Cougar Creek Complex, Oregon–Idaho using the porphyroclast hyperbolic distribution method, and potential use of SC'-type extensional shear bands as quantitative vorticity indicators. Journal of Structural Geology 30, 1005–1012.

Kurz, W., 2005. Constriction during exhumation: evidence from ecologite microstructures. Geology 33, 37–40.

Law, R.D., Knipe, R.J., Dayan, H., 1984. Strain path partitioning within thrust sheets: microstructural and petrofabric evidence from the Moine thrust zone at Loch Eriboll, NW Scotland. Journal of Structural Geology 6, 477–497.

Lin, S., Jiang, D., 2001. Using along-strike variation in strain and kinematics to define the movement direction of curved transpressional shear zones: an example from northwestern Superior Province, Manitoba. Geology 29, 767–770.

Means, W.D., Hobbs, B.E., Lister, G.S., Williams, P.F., 1980. Vorticity and non-coaxiality in progressive deformations. Journal of Structural Geology 2, 371–378.

Peacock, S.M., Norris, P.J., 1989. Metamorphic evolution of the Central Metamorphic belt, Klamath province, California: an inverted metamorphic gradient beneath the Trinity peridotite. Journal of Metamorphic Geology 7, 191–209.

Pfiffner, O.A., Ramsay, J.G., 1982. Constraints on geological strain rates: arguments from finite strain states of naturally deformed rocks. Journal of Geophysical Research 87, 311–321.

Plafker, G., Nokleberg, W.J., Lull, J.S., 1989. Bedrock geology and tectonic evolution of the Wrangellia, Peninsular, and Chugach terranes along the Trans-Alaska Crustal Transect in the Chugach Mountains and southern Cooper River basin. Journal of Geophysical Research 94, 4255–4295.

Platt, J.P., Vissers, R.L.M., 1980. Extensional structures in anisotropic rocks. Journal of Structural Geology 2, 397–410.

Ramsay, J.G., Graham, R.H., 1970. Strain variation in shear belts. Canadian Journal of Earth Sciences 7, 786–813.

Robinson, P., Tucker, R.D., Bradley, D., Berry IV, H.N., Osberg, P.H., 1998. Paleozoic orogens in New England, USA. GFF 120, 119–148.

Schmid, S.M., Fügenschuh, B., Kissling, E., Schuster, R., 2004. Tectonic map and overall architecture of the Alpine orogen. Eclogae Geologicae Helvetiae 97, 93–117.

Schmid, S.M., Pfiffner, O.A., Froitzheim, N., Schönborn, G., Kissling, E., 1996. Geophysical–geological transect and tectonic evolution of the Swiss–Italian Alps. Tectonics 15, 1036–1064.

Simpson, C., De Paor, D.G., 1993. Strain and kinematic analysis in general shear zones. Journal of Structural Geology 15, 1–20.

Snoke, A.W., Barnes, C.G., 2006. The development of tectonic concepts for the Klamath Mountains province, California and Oregon. In: Snoke, A.W., Barnes, C.G. (Eds.), Geological Studies in the Klamath Mountains Province, California and Oregon. Geological Society of America Special Paper, vol. 410, pp. 1–29.

Snoke, A.W., Rowe, D.W., Yule, J.D., Wadge, G., 2001. Petrologic and Structural History of Tobago, West Indies: a Fragment of the Accreted Mesozoic Oceanic-Arc of the Southern Caribbean. In: Geological Society of America, Boulder, Special Paper, vol. 354, p. 54.

Stipp, M., Stünitz, H., Heilbronner, R., Schmid, S.M., 2002. Dynamic recrystallization of quartz: correlation between natural and experimental conditions. In: de Meer, S., Drury, M.R., de Bresser, J.H.P., Pennock, G.M. (Eds.), Deformation Mechanisms, Rheology and Tectonics: Current Status and Future Perspectives. Geological Society, London, Special Publication, vol. 200, pp. 171–190.

Sullivan, W.A., 2008. Significance of transport-parallel strain variations in part of the Raft River shear zone, Raft River Mountains, Utah, USA. Journal of Structural Geology 30, 138–158.

Sullivan, W.A., Law, R.D., 2007. Deformation path partitioning within the transpressional White Mountain shear zone, California and Nevada. Journal of Structural Geology 29, 583–598.

Tikoff, B., Fossen, H., 1995. The limitations of three-dimensional kinematic vorticity analysis. Journal of Structural Geology 17, 1771–1784.

Truesdell, C., 1954. The Kinematics of Vorticity. Indiana University Press, Bloomington, IN, 232 pp.

Tullis, J., Yund, R.A., 1992. The brittle–ductile transition in feldspar aggregates: an experimental study. In: Evans, B., Wong, T.-f. (Eds.), Fault Mechanics and Transport Properties of Rocks. Academic Press, NY, pp. 89–118.

Wright, J.E., 1982. Permo-Triassic accretionary subduction complex, southwestern Klamath Mountains, northern California. Journal of Geophysical Research 87, 3805–3818.

Wright, J.E., Fahan, M.R., 1988. An expanded view of Jurassic orogenesis in the western United States Cordillera: Middle Jurassic (pre-Nevadan) regional metamorphism and thrust faulting within an active arc environment, Klamath Mountains, California. Geological Society of America Bulletin 100, 859–876.

Wright, J.E., Wyld, S.J., 1994. The Rattlesnake Creek terrane, Klamath Mountains, California: an early Mesozoic volcanic arc and its basement of tectonically disrupted oceanic crust. Geological Society of America Bulletin 106, 1033–1056.

Wyld, S.J., Wright, J.E., 1988. The Devil's Elbow ophiolite remnant and overlying Galice Formation: new constraints on the Middle to Late Jurassic evolution of the Klamath Mountains, California. Geological Society of America Bulletin 100, 29–44.

Xypolias, P., Koukouvelas, I.K., 2001. Kinematic vorticity and strain rate patterns associated with ductile extrusion in the Chelmos Shear Zone (External Hellenides, Greece). Tectonophysics 338, 59–77.